In Vivo Mapping of Cholinergic Neurons in the Human Brain Using SPECT and IBVM

David E. Kuhl, Robert A. Koeppe, Jeffrey A. Fessler, Satoshi Minoshima, Robert J. Ackermann, James E. Carey, David L. Gildersleeve, Kirk A. Frey and Donald M. Wieland

Division of Nuclear Medicine, Department of Internal Medicine, University of Michigan Medical Center, Ann Arbor, Michigan

In the search for an in vivo marker of cholinergic neuronal integrity, we extended to human use the tracer (−)-5-[^{123}I]iodobenzovesamicol (IBVM). **Methods:** IBVM, an analog of vesamicol that binds to the acetylcholine transporter on presynaptic vesicles, was prepared with specific activity greater than 1.11×10^9 MBq mmole^{-1}. After intravenous injection of [^{123}I]IBVM, body distribution studies (n = 5) and brain SPECT studies (n = 5) were performed on normal human subjects (n = 10). SPECT images of the brain were collected sequentially over the first 4.5 hr following injection, and again 18 hr later. Data were realigned and transformed to stereotaxic coordinates, and localized activities were extracted for tracer kinetic analysis. The cerebral tracer input function was determined from metabolite-corrected radial arterial blood samples. The best data fit was obtained using a three-compartment model, including terms reflecting cerebral blood volume, exchange of free tracer between plasma and brain and specific binding. **Results:** Dissociation of bound tracer was negligible for up to 4 hr. For the fitted parameters reflecting transport (K_1) and binding site density index (k_3), coefficients of variation were approximately 8% in cortical regions of interest. Relative distributions corresponded well with postmortem immunohistochemical values reported for the acetylcholine-synthesizing enzyme choline acetyltransferase, k_3 (IBVM binding site density index), and tracer activity distribution at 22 hr, but not at 4 hr after injection. **Conclusion:** SPECT imaging of [^{123}I]IBVM succeeds as an in vivo measure of cholinergic neuronal integrity and should be useful for the study of cerebral degenerative processes such as Alzheimer's disease.

Key Words: iodobenzovesamicol; cholinergic neurons, in vivo mapping of; SPECT

J Nucl Med 1994; 35:405–410

In the search for an in vivo marker of cholinergic neuronal integrity, we extended to human use the tracer (−)-5-[^{123}I]iodobenzovesamicol (IBVM). IBVM is an analog of vesamicol, which binds to the acetylcholine transporter in presynaptic vesicles (*1–3*). In mouse brain, IBVM is a stereospecific, regionally specific ligand which marks the presynaptic cholinergic vesicle site (*4,5*). There is need for a valid and noninvasive means to map presynaptic cholinergic integrity in the living human brain, especially in the study of normal aging and dementing disorders. This has led recently to careful examination of new PET agents (*6–9*) and SPECT agents (*4,5,10,11*) with potential for this purpose. We report here the successful application in human subjects of the recently proposed SPECT agent, [^{123}I]IBVM (*4,5,11*), as an in vivo marker of presynaptic cholinergic terminals, which suggests that this method should be useful as a measure of cholinergic neuronal integrity in evaluating cerebral degenerative processes such as aging and Alzheimer's disease.

METHODS

IBVM was prepared for human use by oxidative radioiodination of the respective (−)-5-tributyltin precursor (*11*). The tributyltin precursor was prepared from (−)-5-[^{127}I]IBVM, which was synthesized as previously described (*4*). Purification of the crude reaction product was accomplished by HPLC using a C18 minibore column and tandem micro-volume flow cells coupled to UV and radiation detectors. Specific activity of the product was greater than 1.11×10^9 MBq mmole^{-1} (30,000 Ci/mmole) as determined by HPLC/UV analysis at 210 nm of a known amount of radioactivity (700–1000 MBq); reference was then made to a HPLC/UV standard curve of 5-IBVM at 210 nm. The radiotracer was injected as a sterile, pyrogen-free solution in ammonium acetate-buffered bacteriostatic saline containing 10% ethyl alcohol by volume.

First, body distribution was studied in five healthy subjects (23–37 yr old), after which brain SPECT was performed in another five healthy subjects (22–29 yr old). In order to minimize iodine uptake in the thyroid gland, each subject was given oral Lugol's solution (one drop three times daily) for one day prior and for three days after intravenous injection of IBVM (370 MBq). In addition, the SPECT group was administered an oral laxative (Dulcolax®; CIBA, Summit, NJ) one day after the IBVM injection, in order to reduce radiation exposure to the bowel.

In the first group of subjects, IBVM was injected, body activity distribution was imaged at intervals with a scintillation camera, and urine and feces were collected over a 48-hr period. Arterial blood samples were withdrawn to determine a tracer time-activity curve.

Adult human absorbed dose was calculated following the MIRD formalism (*12*). Radiopharmacokinetic data for organs (percentage administered activity per organ versus time) was estimated from rat dissection and human excretion data. Three

Received Jul. 14, 1993; revision accepted Dec. 10, 1993.

For correspondence or reprints contact: David E. Kuhl, MD, Division of Nuclear Medicine, University of Michigan Medical Center, Ann Arbor, MI 48109-0028.

female and three male Sprague-Dawley rats were studied at five time points with 18 organs sampled at each point. Organ residence times were calculated and entered into the MIRDOSE program (*13*). The ICRP gastrointestinal tract model (*14*) was used to calculate the absorbed dose to the intestines. For the urinary bladder wall, the dynamic bladder model (*15*) was used assuming a 3.5-hr filling and voiding interval. The absorbed dose to the gallbladder wall was calculated assuming a 6-hr bladder filling and emptying interval.

In the second group of subjects, SPECT (Prism 3000; Picker International, Cleveland, OH) images of the brain were collected sequentially over the first 4.5 hr and then again at 22 hr after the IBVM injection. To compensate for attenuation, a first-order Chang correction algorithm was applied using operator-determined sets of ellipses defined on the transverse images. Spatial resolution (FWHM) in the transverse plane was 12.5 mm (central axis) and 8.5 mm (tangential).

To determine the cerebral tracer input function, radial arterial blood was sampled and corrected for metabolites. Human blood samples (1 ml) were taken for metabolic analysis at the following seven time points after intravenous injection of [^{123}I]IBVM: 3, 10, 60, 120, 180 and 270 min, and 22.5–24 hr. The blood samples were centrifuged for 1 min at 16,000 G; 250 μl of plasma were transferred to a clean vial and mixed with 750 μl of 0.1 *M* ammonium acetate that had been spiked with unlabeled 5-IBVM and potassium iodide (10 μl of a solution of 10 μg of each compound in 10 ml of absolute ethanol). Each diluted plasma sample was transferred to a preconditioned C18 Sep-Pak Cartridge (Millipore Corporation, Milford, MA) and eluted consecutively with 5 ml of ethanol/0.1 *M* ammonium acetate of the following proportions: 40/60, 40/60, 95/5, 95/5. The void volume fraction (fraction 1) plus the 5-ml fractions that were collected were counted on a Packard 5780 Autogamma Counter. Metabolites eluted in fractions 1–3; unchanged [^{123}I]IBVM eluted in fractions 4 and 5.

SPECT data were collected as a sequence of 26 frames over a 4.5-hr period after injection. This sequence included ten 2-min scan frames for the first 20 min, seven 10-min frames continuing out to 90 min, three 10-min frames from 2.0–2.5 hr, three 10-min frames from 3.0–3.5 hr, and finally three 10-min frames from 4.0–4.5 hr postinjection. This was followed at 22 hr by a final 1-hr set of six 10-min scan frames. In the data analysis, head motion was corrected using fiducial makers in each set of frames, separately for Days 1 and 2. Then, the first frame of Day 2 was co-registered to the last frame of Day 1 using an automated method that matches two image sets by maximizing image similarity. Then, the rest of the frames on Day 2 were transformed to the same orientation as the last frame of Day 1. The intercommissural (AC-PC) line was estimated by an automated method applied to a summation image of early uptake (*16,17*), and all frames were transformed to a stereotactic coordinate system according to the AC-PC line. Each stereotactic frame consisted of 40 slices with uniform voxel size of 4.45 mm. Multiple voxels of interest (VOI) (4 ml) were localized stereotactically in selected brain structures on the summation image of early uptake and then were applied to each of the dynamic sequence of 32 stereotactic scan frames. Sequential VOI values from frames 1 through 26 (0–4.5 hr postinjection) were used for the tracer kinetic estimation.

RESULTS

Body Distribution and Dosimetry

After [^{123}I]IBVM injection, we recorded no respiratory distress or any other pharmacological response. Decay-corrected activity peaked in liver, lung and brain during the first 10 min, declined by half at 4 hr and subsequently declined at a lesser rate over the next day. Activity appeared promptly in the gallbladder and moved through the intestine (Figs. 1, 2).

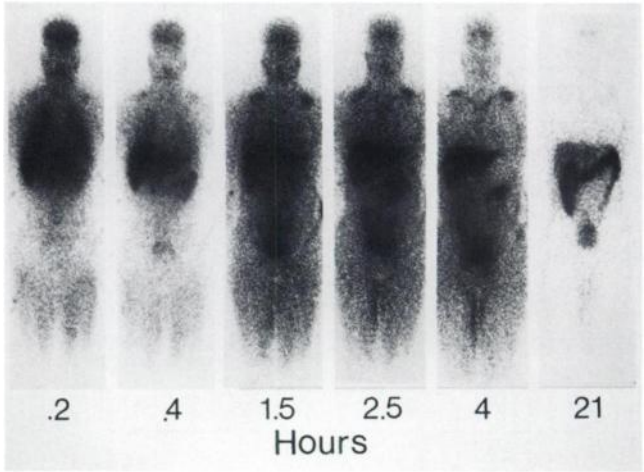

FIGURE 1. Human body distribution of activity after intravenous injection of IBVM. Uptake peaks early in liver, lung and brain, then declines steadily, as gallbladder and intestinal activity appear.

Absorbed dose estimates are summarized in Table 1. The "critical" organs for [^{123}I]IBVM are the gallbladder and the intestinal tract. From the human excretion studies, it was determined that approximately 70% of the administered activity was excreted to the small intestine, while 12% was excreted to the urinary bladder with a biological half-life of 8 hr and 15% with a biological half-life of 0.15 hr. Twenty-one percent of the administered activity was assumed to pass through the gallbladder. Activity in the intestinal tract was the primary contributor to the absorbed dose to the ovaries and the red marrow. In practice, the absorbed dose to the thyroid and the intestinal tract were reduced by the use of Lugol's solution and laxatives.

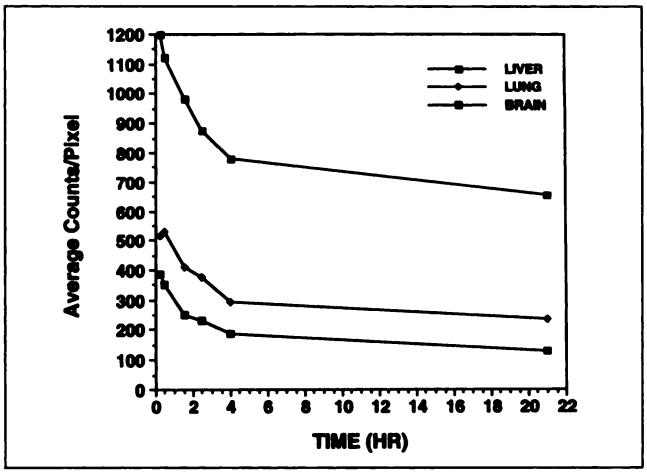

FIGURE 2. Time course of activity concentration in human liver, lung and brain after intravenous IBVM.

TABLE 1
Absorbed Dose Estimates for the Adult Human from Single Intravenous Administration of [^{123}I]IBVM

Organ	Absorbed Dose (μGy MBq^{-1})	(s.d.*)
Brain	3.4	(0.5)
Gallbladder wall	180	
GI tract		
Small intestine	110	
Upper large intestine	280	
Lower large intestine	310	
Liver	17.8	(1.1)
Lungs	3.5	(0.3)
Ovaries	70.1	(4.5)
Red marrow	11	
Testes	21.6	(3.3)
Thyroid (unblocked)	20.4	(15.7)
Urinary bladder wall	56	
Total body	11.5	(0.2)

*Standard deviation from animal source organ data.

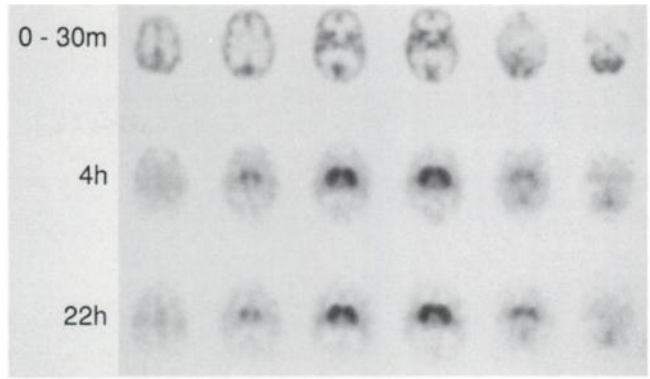

FIGURE 3. SPECT images of the human brain with respect to time after intravenous IBVM injection. The pattern of activity distribution resembles relative perfusion in the earliest images, then progressively striatal concentration dominates. At 22 hr after injection, the relative distribution of count density and IBVM binding site density index are similar. (Imaging duration: top row 20 min; mid row 30 min; bottom row 60 min.)

Blood Curve and Metabolites

The time course of IBVM in arterial plasma following rapid intravenous injection demonstrated the typical abrupt rise and rapid initial clearance of tracer for the first several minutes, followed by a long progressively slower clearance as recirculation effects occurred. IBVM was found to metabolize quite rapidly. At 10 min postinjection, the fraction of authentic IBVM radioactivity in plasma averaged 79% across the five subjects (range 75%–86%). By 30 min postinjection, the authentic fraction in plasma had decreased to 47% (range 36%–58%). By 1 hr, the fraction averaged only 30%, ranging from 21% to 36% across subjects. From 2–4 hr postinjection, the authentic IBVM fraction dropped more slowly, decreasing to 16% (range 12%–21%) by the end of the 4.5-hr dynamic scanning period.

Brain Tomography

The earliest SPECT images demonstrated a radioactivity distribution resembling cerebral perfusion, but by 4 hr after injection striatal activity dominated. This appearance was maintained at 22 hr postinjection (Fig. 3). Tracer kinetic estimates were performed using two- and three-compartment models (*18,19*) (Fig. 4). The two-compartment model, estimating ligand transport (K_1), total ligand distribution volume (DV) and cerebral blood volume (CBV) did not describe the in vivo radioactivity time course well, thus yielding poor fits, as IBVM does not equilibrate rapidly enough to satisfy assumptions of such a model configuration. Kinetic estimation of K_1, k_2, k_3 (rate constant for binding to vesicular transporter, reflecting binding site density), k_4 (rate of release from vesicle) and CBV using a three-compartment configuration produced significantly better fits than the two-compartment configuration. Fitted k_4 values were consistently near zero for all regions examined, with group values ranging from 0.002 ± 0.001 min^{-1} in striatum to 0.003 ± 0.001 min^{-1} in cortex. These small values in conjunction with the relatively high coefficients of variation suggested the adoption of a three-compartment model estimating K_1, k_2, k_3 and CBV, thus simplifying the fitting procedure in order to reduce variability in the parameter estimates. Goodness of fit was not significantly reduced for striatal regions and was marginally, but consistently, reduced for cortical regions. However, in reducing the number of fitted parameters by one, the coefficients of variation decreased across subjects for the fitted parameters of the various ROIs. Further analysis of both a greater number of subjects and different subject populations (age and disease groups) will be required before we can determine the best trade-off between bias and variability in the parameter estimates, and therefore whether or not to include a fitted or fixed value of k_4 in the model. For the results reported in this initial study, we adopted the

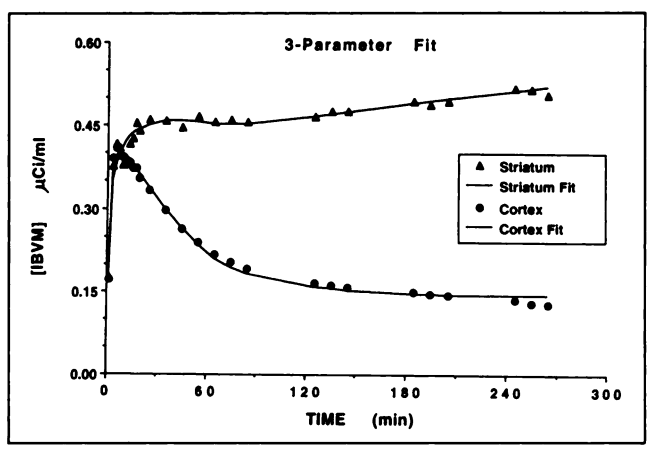

FIGURE 4. Time course of SPECT-determined radioactivity (μCi ml^{-1}) in the striatum and cortex from one of the five normal subjects. The solid lines show the best fit to the data using a three-compartment model to estimate K_1, k_2, k_3 and CBV (k_4 = 0).

TABLE 2
IBVM Kinetics

Region	Transport				Binding site density index	
	K_1 (ml/g/min) (mean ± s.d.)	(COV)	k_2 (min^{-1}) (mean ± s.d.)	(COV)	k_3 (min^{-1}) (mean ± s.d.)	(COV)
Striatum	0.116 ± 0.008	6.5%	0.0165 ± 0.033	20.3%	0.1021 ± 0.0157	15.4%
Thalamus	0.127 ± 0.012	9.8%	0.0306 ± 0.0048	15.8%	0.0304 ± 0.0037	12.3%
Hippocampus	0.096 ± 0.007	7.7%	0.0274 ± 0.0042	15.5%	0.0224 ± 0.0073	32.8%
Pons	0.106 ± 0.019	17.8%	0.0284 ± 0.0049	17.4%	0.0204 ± 0.0035	17.0%
Cerebellar vermis	0.118 ± 0.011	9.1%	0.0285 ± 0.0031	10.9%	0.0187 ± 0.0034	18.0%
Temporal cortex	0.115 ± 0.010	8.4%	0.0335 ± 0.0044	13.1%	0.0151 ± 0.0014	9.3%
Cerebellar hemisphere	0.131 ± 0.023	17.6%	0.0347 ± 0.0049	14.1%	0.0147 ± 0.0035	23.8%
Parietal cortex	0.118 ± 0.009	7.9%	0.0368 ± 0.0039	10.5%	0.0130 ± 0.0004	3.3%
Frontal cortex	0.114 ± 0.009	8.3%	0.0346 ± 0.0041	11.7%	0.0128 ± 0.0007	5.8%
Occipital cortex	0.113 ± 0.009	8.3%	0.0367 ± 0.0036	9.7%	0.0107 ± 0.0007	6.2%

three-compartment model fitting K_1, k_2, k_3 and blood volume, ($k_4 = 0$).

Fitted values for the transport rate parameter, K_1, employing total plasma IBVM as the input function, varied from 0.096 to 0.131 ml g^{-1} min^{-1} across regions. Estimates of k_3, the rate constant for binding to the vesicular transporter, ranged from a mean of 0.102 min^{-1} in striatum to 0.013 min^{-1} in cortex with coefficients of variation of approximately 8% in cortical regions of interest (Table 2). Assuming normal blood flow, the extraction fraction of IBVM is approximately 15%. Ultrafiltration analyses indicate that 90%–95% of plasma IBVM is protein bound. Thus, the extraction estimate indicates that a substantial portion of IBVM entering brain is derived from the protein-bound pool. Group mean estimates of k_2 ranged from 0.017 min^{-1} in the striatum to 0.042 min^{-1} in the occipital cortex. The ratio K_1/k_2, representing the distribution volume of the rapidly equilibrating tissue compartment, ranged from about 3.0–3.5 in cortical regions to about 6.0–7.0 in the basal ganglia. The larger DV in the striatum, where greater binding occurs, may be caused by the inability of the kinetic model to separate completely the specific compartment from the free plus nonspecific compartment. The ratio of binding-to-clearance (k_3/k_2) was about eight times higher in striatum than in cortex. Mean fitted cerebral blood volume fractions across subjects ranged from 0.027 ml g^{-1} (2.7%) in white matter, 0.035–0.040 ml g^{-1} in the cortex, to a maximum of 0.047 ml g^{-1} in the putamen. These values are consistent with the known range of CBV in humans.

There was consistency among the relative distributions of k_3, the binding site density index, radiotracer activity distribution at 22 hr after injection, and the regional distributions for postmortem immunohistochemical values reported in the human brain (*20–22*) for the acetylcholine synthesizing enzyme choline acetyltransferase (ChAT), an established presynaptic cholinergic neuronal marker (Table 3). For example, striatum-to-cortex ratios corresponded well for ChAT (7.8–15.6), k_3 (IBVM binding site density index) (8.0) and tracer activity distribution at 22 hr (6.6), but not at 4 hr (3.8). The correspondence for rank order of these neuronal marker distributions is [striatum] ⋙ [thalamus, hippocampus, pons, cerebellar vermis] > [temporal/cerebellar/parietal/frontal cortex] > [occipital cortex] (Table 3).

TABLE 3
Regional Measures Related to Frontal Cortex

Region	IBVM Scan			Postmortem ChAT*		
	k_3	Count density 4 hr	Count density 22 hr	McGeer 1980	Bird 1983	Araujo 1988
Striatum	8.0	3.8	6.8	15.6	14.0	7.8
Thalamus	2.4	2.0	2.6	1.1		4.9
Hippocampus	1.7	1.5	1.9	1.2	1.3	2.6
Pons	1.6	1.4	1.5	2.1		
Cerebellar vermis	1.5	1.5	1.5	1.0		
Temporal cortex	1.2	1.1	1.2		1.1	1.2
Cerebellar hemisphere	1.1	1.1	0.9	0.5	1.1	
Parietal cortex	1.0	1.0	1.0			1.1
Frontal cortex	1.0	1.0	1.0	1.0	1.0	1.0
Occipital cortex	0.8	0.8	0.7	0.5		0.6

*ChAT ratios are calculated from published data (*18–20*).

DISCUSSION

IBVM is a structural analog of vesamicol (*4*), a compound shown to be a stereoselective, noncompetitive inhibitor of acetylcholine uptake into presynaptic cholinergic vesicles, where it binds with high affinity at or near to the vesicular acetylcholine transporter (*1–3*). IBVM has late retention in mouse or rat brain, which matches the distribution of the established presynaptic cholinergic marker ChAT (*4,5*), evidence that confirms the role of IBVM as a specific cholinergic neuron marker. The human studies reported here give further confirmation.

Cholinergic innervation has been localized in macaque and rat brains by means of ChAT immunohistochemistry and acetylcholinesterase histochemistry (*23*). Cholinergic innervation is most dense in the striatum, due to the presence of local cholinergic interneurons. Lesser concentrations are found in the cortex, amygdala and hippocampus, the terminating sites for projections from the basal forebrain cholinergic nuclei. Still lesser concentrations occur in the thalamus, which is the terminus for ascending projections from cholinergic nuclei in the pontomesencephalic reticular formation (*23*). Corresponding studies of postmortem human brain are more limited (*20–22*).

Distributions were similar for our SPECT-determined binding of IBVM and ChAT activity reported for postmortem human brain (*20–22*). Due to a high density of cholinergic interneuron terminals in striatum, IBVM binding and ChAT activity were highest there, and much less in cortex, where the terminals of projections from the basal forebrain cholinergic system are less concentrated. There was further agreement among intermediate density sites for rank order of these two marker distributions (Table 3) in spite of SPECT distortions due to partial volume effects and wide variations among laboratories in parametric measures published for ChAT activity in postmortem human brain.

In the cerebellum, markers for presynaptic cholinergic neurons are relatively more dense in human brain than in mouse or rat brain. For example, the value of the cerebellum-to-cortex ratio from published data is 0.11 for ChAT activity in rat brain (*24*) and 0.09 for IBVM binding in mouse brain (*4*). But in human brain, the values for this ratio are reported as 0.5 or 1.1 for ChAT activity (*20,21*), results which agree with the value of 1.1 that we found for IBVM binding determined with SPECT.

Although IBVM is a highly toxic curaremimetic, the high specific activity of the tracer permitted a safe subpharmacologic dose to be used. Assuming a minimum specific activity of 1.11×10^9 MBq $mmole^{-1}$, 370 MBq of IBVM administered to a 50-kg person is equivalent to 2.9 ng/kg of carrier, which is 25,000 times less than the IBVM dose of 75–150 μg/kg, which produces lethargy and is 75,000 times less than the LD_{50} of 218 μg/kg in Sprague-Dawley rats (*11*) (Kostyniak PJ, Jung YW, Wieland DM, Kuhl DE. Lethargy induction and LD_{50}, unpublished findings, 1991).

The similarity of the binding site density index (k_3) distribution and relative activity distribution at 22 hr makes a single late imaging session a potential alternative to the full kinetic analysis of early time course imaging. However, k_3 determination gives a regional assessment of binding site density without requiring reference to other parts of the brain which then must be presumed to have normal binding densities.

We conclude that SPECT imaging of [^{123}I]IBVM succeeds in human subjects as an in vivo measure of presynaptic cholinergic terminal density. Consequently, this method should be useful as a measure of cholinergic neuron integrity in studies of aging and Alzheimer's disease.

ACKNOWLEDGMENTS

This project was supported in part by U.S. Public Health service grants RO1 NS24896, RO1 NS25656, T32 CA09015 and MO1RR00042 and Department of Energy research grant #DE-FG02-87ER60561. Dr. Fessler was supported in part under the Department of Energy Alexander Hollaender Distinguished Postdoctoral Fellowship Program. We thank Edward P. Ficaro, PhD, Clarke A. Hagen, MS, Sunil Mukhopadhyay, PhD, Neil A. Petry, MS, Steven R. Pitt, BS and Phillip Sherman, BS for technical assistance; Nancy E. Lowenbergh, BSN for subject recruitment; Olga Mancik and Karen Kreutzer for typing the manuscript; and the Phoenix Memorial Laboratory of the University of Michigan for use of their radiochemistry facilities.

REFERENCES

1. Marien MR, Parsons SM, Altar CA. Quantitative autoradiography of brain binding sites for the vesicular acetylcholine transport blocker 2-(4 phenylpiperidino)cyclohexanol (AH5183). *Proc Natl Acad Sci* 1987;84:876–880.
2. Altar CA, Marien MR. [^{3}H]Vesamicol binding in brain: autoradiographic distribution, pharmacology, and effects of cholinergic lesions. *Synapse* 1988;2:486–493.
3. Rogers GA, Parsons SM, Anderson DC, et al. Synthesis, in vitro acetylcholine-storage-blocking activities, and biological properties of derivatives and analogues of trans-2-(4-phenylpiperidino)cyclohexanol (Vesamicol). *J Med Chem* 1989;32:1217–1230.
4. Jung Y-W, Van Dort M, Gildersleeve DL, Wieland DM. A radiotracer for mapping cholinergic neurons of the brain. *J Med Chem* 1990;33:2065–2068.
5. Jung Y-W, Van Dort ME, Gildersleeve DL, Wieland DM, Kuhl DE. Structural and preclinical studies with the radioiodinated cholinergic neuron marker (−)-5-iodobenzovesamicol. *Soc Neurosci Abstr* 1991;17:724.
6. Kilbourn MR, Jung Y-W, Haka MS, Gildersleeve DL, Kuhl DE, Wieland DM. Mouse brain distribution of a carbon-11-labeled vesamicol derivative: presynaptic marker of cholinergic neurons. *Life Sci* 1990;47:1955–1963.
7. Mulholland GK, Jung Y-W. Improved synthesis of [^{11}C]methylaminobenzovesamicol. *J Lab Cmpds Radiopharm* 1992;31:253–259.
8. Widen L, Eriksson L, Ingvar M, Parsons SM, Rogers GA, Stone-Elander S. Positron emission tomographic studies of central cholinergic nerve terminals. *Neurosci Lett* 1992;136:1–4.
9. Mulholland GK, Jung Y-W, Wieland DM, Kilbourn MR, Kuhl DE. Synthesis of [^{18}F]fluoroethoxybenzovesamicol, a radiotracer for cholinergic neurons. *J Lab Cmpds Radiopharm* 1993;33:583–592.
10. Efange SMN, Dutta AK, Michelson RH, et al. Radioiodinated 2-hydroxy-3-(4-iodophenyl)-1-(4-phenylpiperidinyl)propane—potential radiotracer for mapping central cholinergic innervation in vivo. *Nucl Med Biol* 1992;19:337–348.
11. Van Dort ME, Jung Y-W, Gildersleeve DL, Hagen CA, Kuhl DE, Wieland DM. Synthesis of the ^{123}I- and ^{125}I-labeled cholinergic nerve marker (−)-5-iodobenzovesamicol. *Nucl Med Biol* 1993;20:929–937.
12. Loevinger R, Berman M. A revised schema for calculating the absorbed dose from biologically distributed radionuclides. *MIRD Pamphlet no. 1, revised*. New York: Society of Nuclear Medicine; 1976.
13. Watson E, Stabin M, Bloch W. *MIRDOSE (version 2)*. Oak Ridge Associated Universities; 1984.

14. ICRP. Limits for intakes of radionuclides by workers. *ICRP Publication 30*. Oxford: Pergamon; 1979.
15. Cloutier RJ, Smith SA, Watson EE, Snyder WS, Warner GG. Dose to the fetus from radionuclides in the bladder. *Health Phys* 1973;25:147–161.
16. Minoshima S, Berger KL, Lee KS, Mintun MA. An automated method for rotational correction and centering of three-dimensional functional brain images. *J Nucl Med* 1992;33:1579–1585.
17. Minoshima S, Koeppe RA, Mintun MA, et al. Automated detection of the intercommissural (AC-PC) line for stereotactic localization of functional brain images. *J Nucl Med* 1993;34:322–329.
18. Koeppe RA. Compartmental modeling alternatives for kinetic analysis of PET neurotransmitter/receptor studies. In: DE Kuhl, ed. *Frontiers in nuclear medicine: in vivo imaging of neurotransmitter functions in brain, heart, and tumors*. Washington, DC: American College of Nuclear Physicians; 1990:113–139.
19. Koeppe RA, Frey KA, Mulholland GK, Kilbourn MR, Buck A, Lee KS, Kuhl DE. [^{11}C]tropanyl benzilate binding to muscarinic cholinergic receptors: methodology and kinetic modeling alternatives. *J Cereb Blood Flow Metab* 1994;14:85–99.
20. McGeer PL, Eccles SJC, McGeer EG. *Molecular neurobiology of the mammalian brain*. New York: Plenum Press; 1980:150.
21. Bird TD, Stranahan S, Sumi SM, Raskind M. Alzheimer's disease: choline acetyltransferase activity in brain tissue from clinical and pathological subgroups. *Ann Neurol* 1983;14:284–293.
22. Araujo DM, Lapchak PA, Robitaille Y, Gauthier S, Quirion R. Differential alteration of various cholinergic markers in cortical and subcortical regions of human brain in Alzheimer's disease. *J Neurochem* 1988;50:1914–1923.
23. Mesulam MM, Mufson EJ, Wainer BH, Levey AI. Central cholinergic pathways in the rat: An overview based on an alternative nomenclature (Ch1–Ch6). *Neuroscience* 1983;10:1185–1201.
24. Stavinoha WB, Weintraub ST, Modak AT. Regional concentrations of choline and acetylcholine in the rat brain. *J Neurochem* 1974;23:885.

(continued from page 5A)

FIRST IMPRESSIONS

Bone Scan of Feet Affected by Urinary Incontinence

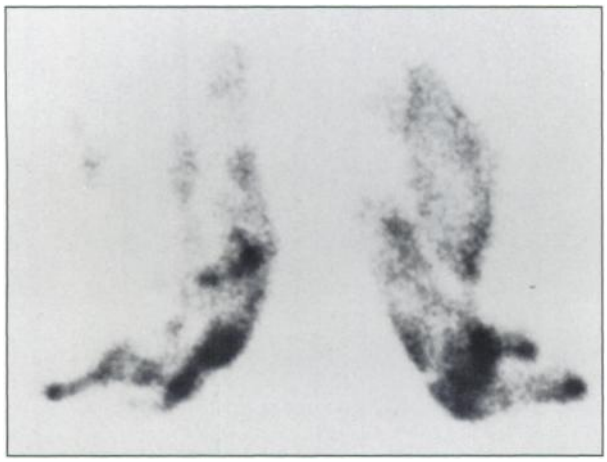

FIGURE 1.

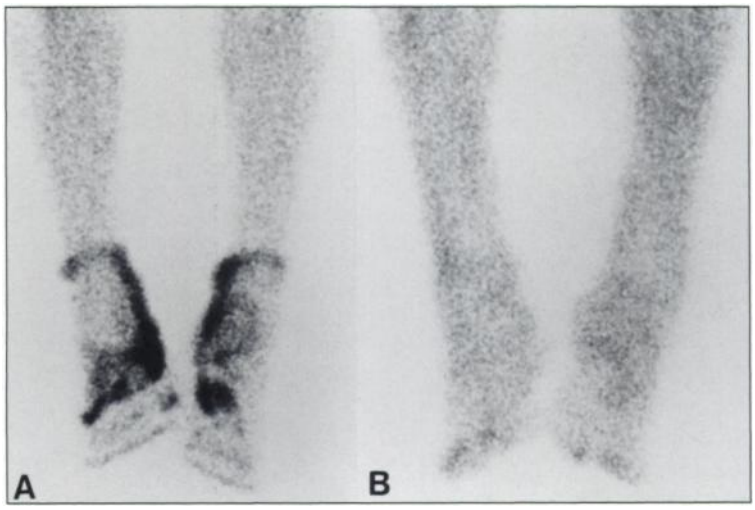

FIGURE 2.

PURPOSE
A 75-yr-old white male with a history of urinary incontinence, dysuria and prostate carcinoma was referred for a bone scan as part of a metastatic workup. Figure 1, a scan of the patient's socks contaminated with radioactive urine, illustrates the "hot sock sign" of urinary incontinence (*1*). Figure 2 is an anterior view of the feet with socks (A) and without socks (B).

TRACER
Technetium-99m-MDP

ROUTE OF ADMINISTRATION
Intravenous

TIME AFTER INJECTION
3 hr

INSTRUMENTATION
Siemens whole-body camera with a high-resolution collimator

CONTRIBUTORS
Shobha Desai and David Yuille

INSTITUTION
St. Luke's Medical Center, Milwaukee, Wisconsin

REFERENCE
1. Wells DL, Bernier DR. Puss-in-Boots. In: *Radionuclide imaging artifacts*. Chicago: Yearbook Medical Publishers; 1980:98.